


Sequential Synchronous Mechanism for Double-Electron Capture: Insights into Unforeseen Large Cross Sections in Low-Energy $\text{Sn}^{3+} + \text{H}_2$ Collisions

Lamberto Oltra¹, Luis Méndez¹, and Ismanuel Rabadán^{1*}

Laboratorio Asociado al CIEMAT de Física Atómica y Molecular en Plasmas de Fusión, Departamento de Química, Universidad Autónoma de Madrid, C/ Francisco Tomás y Valiente 7, 28049-Madrid, Spain

Klaas Bijlsma², Emiel de Wit², and Ronnie Hoekstra²

Zernike Institute for Advanced Materials, University of Groningen, Nijenborgh 4, 9747 AG Groningen, The Netherlands and Advanced Research Center for Nanolithography (ARCNL), Science Park 106, 1098 XG Amsterdam, The Netherlands

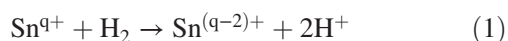
 (Received 16 July 2024; revised 30 September 2024; accepted 3 December 2024; published 7 March 2025)

Remarkably large double electron capture cross sections, on the scale of 10^{-15} cm², are observed in low-energy (< 50 eV/u) collisions between Sn^{3+} and H_2 . Given that the reaction is energetically highly unfavorable, one would expect negligibly small cross sections. Through the propagation of vibrational wave packets on coupled multiple potential energy surfaces, a novel charge transfer mechanism, driven in tandem by ion motion and molecular vibration, is revealed, offering insights into the unusual energy dependence of the measured cross sections.

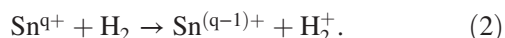
DOI: [10.1103/PhysRevLett.134.093002](https://doi.org/10.1103/PhysRevLett.134.093002)

Tin plasmas are emerging as a focal point in atomic physics research because of their potential applications, such as vapor shielding in Tokamak devices [1–3], and their established role as intense sources of 13.5 nm extreme ultraviolet (EUV) light, driving cutting-edge EUV nanolithography tools [4–7]. In this last application, besides the desired EUV light, the plasma emits energetic multiply charged tin ions [8–10]. To prevent these ions to reach and possibly damage the intricate EUV optics of the plasma chamber, the plasma is embedded within a H_2 gas [11,12].

Two electronic processes play a significant role in the charge-state lowering of the tin ions and, indirectly, in the mitigation of multiply charged ions escaping the plasma. These are double electron capture (DEC):



and single electron capture (SEC):



The work of Rai *et al.* [13] showed that the initial steps of charge state lowering of energetic tin ions happens rapidly, leading to a charge state distribution peaking near $q = 3$.

*Contact author: ismanuel.rabadan@uam.es

Published by the American Physical Society under the terms of the [Creative Commons Attribution 4.0 International license](https://creativecommons.org/licenses/by/4.0/). Further distribution of this work must maintain attribution to the author(s) and the published article's title, journal citation, and DOI.

Subsequent steps from Sn^{3+} determine the final distribution of doubly and singly charged ions.

In this Letter, we focus on DEC reactions by Sn^{3+} ions, which provide another route to produce Sn^+ ions next to the SEC cascade (Sn^{3+} , Sn^{2+} , Sn^+). This is particularly important since, according to measurements by Abramenko *et al.* [14], Sn^+ ions have larger stopping cross sections than Sn^{2+} ones at energies above 3 eV/u.

DEC in ion collisions with molecules is typically understood to occur while the molecule remains in, or close to, its equilibrium geometry, with both electrons being transferred to the projectile ion. Under these conditions, DEC by Sn^{3+} ions from H_2 would be endoergic by no less than 6 eV. As a result, the cross sections at low collisions energies would be extremely small, on the order of 10^{-17} cm², compared to the typical 10^{-15} cm² of exothermic reactions. This aligns with a well-established feature of endoergic collision systems (see, e.g., Refs. [15–17]): they generally exhibit low cross sections at lower energies and an increase with rising collision energy. However, our experiments reveal an unexpected and striking deviation from this behavior. The DEC cross sections are not negligibly small; instead, they are remarkably large and display the opposite energy dependence, growing larger at lower energies. To account for this surprising result, we propose a two-step charge transfer mechanism: first, the transfer of one electron from the neutral molecule to the ion at long projectile-target distances, and second, the capture of the second electron by the projectile at shorter distances, facilitated by the bond stretching of H_2^+ during the time between the two capture events.

DEC experimental data are obtained through crossed-beam experiments with a Sn^{3+} ion beam and H_2 gas jet. The ion beam is generated with the Zernike low-energy ion beam facility (ZERNIKELEIF) with ions from an electron cyclotron resonance ion source, as described by Rai *et al.* [18]. The experimental setup is floating on a set elevated potential, thereby decelerating incoming ions to a desired collision energy. After traversing the gas target, where the Sn ions may have captured one or both electrons from a hydrogen molecule, the Sn ions are collected and analyzed by a retarding field analyzer (RFA). By setting appropriate retarding voltages, the 3+, 2+, and 1+ charge states are blocked cumulatively. From the measured currents at these voltages, the cross sections for SEC and DEC can be determined. To correct for secondary collisions, the measurements are performed at three values of target density and the extracted cross sections are extrapolated to zero pressure. To obtain absolute cross sections, the setup is calibrated against cross sections for O^{6+} ions colliding with H_2 molecules reported by Machacek *et al.* [19]. An extensive description of the experimental setup and procedure can be found in [20], Chap. 4.

Previous theoretical studies [21–26] of ion collisions with H_2 , carried out within the Franck-Condon approximation (FCA) framework, have shown that DEC cross sections are of similar magnitude to SEC ones only when the energy differences between the electronic states involved are comparable, and that DEC cross sections increase with the impact energy of the projectile, in agreement with experimental works [27–32]. At low collisional energies, some discrepancies between experiment and theory were pointed out [27,31]. Giese *et al.* [33] carried out a detailed experimental study of DEC in Ar^{5+} collisions with H_2 at low energies and suggested that the molecular bond length increases during the capture process. This observation questioned the use of the FCA. In the framework of the molecular description of the collisional process, Giese *et al.* recognized the need to employ potential energy surfaces that depend on both the projectile-target distance and the molecular bond length, rather than relying solely on one-dimensional curves, to fully comprehend the physics at play. Since then, theoretical modeling of DEC at low impact energies has been limited. Notable attempts include the five-body classical Monte Carlo calculations by Wood and Olson [34] and DuBois *et al.* [35]. These studies confirmed the need to go beyond the FCA.

In this Letter, we propose a sequential synchronous mechanism for DEC. In a first step, the projectile captures one electron from the neutral target at large distances; in the adiabatic molecular picture, this first event takes place at narrow avoided crossings. At that moment, the target is close to its equilibrium geometry because the perturbation induced by the ion field is still small, and the FCA is still valid. The removal of the first electron sets the target out of

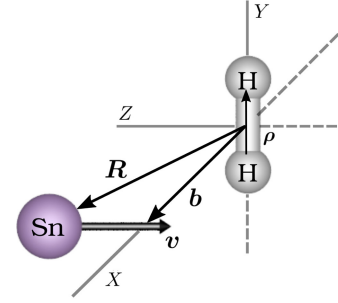


FIG. 1. Scheme of the collision geometry considered in this Letter: The tin ion moves in a rectilinear trajectory with impact parameter b and velocity v , both perpendicular to the hydrogen internuclear vector ρ .

its equilibrium geometry, triggering the molecular motion while the projectile continues in its trajectory. The second electron is captured at short projectile-target distances, where the perturbation of the projectile on the charged target is large and when the target is vibrationally excited due to the first electron removal. The capture of the second electron requires the synchronization of two motions: the projectile along its trajectory and the internal nuclear motion of the target. In this second event, the FCA is not expected to be valid.

Our model considers that the projectile follows a straight line trajectory, $\mathbf{R} = \mathbf{b} + \mathbf{v}t$, with \mathbf{b} , the impact parameter vector, and \mathbf{v} the velocity one, both perpendicular to the H-H internuclear vector, ρ , as shown in Fig. 1: the molecule is always perpendicular to the ion trajectory and the system maintains the C_{2v} symmetry. In the following, we take into account that the electronic wave functions are calculated in a rotating reference frame $\tilde{X}, \tilde{Y}, \tilde{Z}$, with $\tilde{Y} = Y$ and $\tilde{Z} \parallel \mathbf{R}$. At the closest approach point, $\tilde{Z} \parallel \mathbf{b}$ and $\tilde{X} \parallel \mathbf{v}$. Accordingly, the Sn orbitals p_z, p_x belong to A_1 and B_1 irreducible representations, respectively.

The potential energy curves (PECs) of the electronic states of the $(\text{Sn} + \text{H}_2)^{3+}$ system are illustrated in Fig. 2 as functions of ρ for fixed $R = 5$ bohr. The DEC channel (V) appears in both the A_1 and B_1 subsystems and its asymptotic configuration (large ρ) is $\text{Sn}^+(5s^25p^2P^0) + 2\text{H}^+$; it is adiabatically connected with (I) in the A_1 symmetry, a state resembling the initial configuration (the target molecule is neutral), and with the SEC state (II) $\text{Sn}^{2+}(5sp_x^3P^0) + \text{H}_2^+(X^2\Sigma_g^+)$, in the B_1 symmetry. The potential well of the SEC state in the B_1 symmetry (II) is shallower than those of the entrance channel (I) and the SEC state (III) in the A_1 subsystem because the interaction between the p_x orbital of Sn and σ_g of H_2 vanishes, while it is not zero between p_z and σ_g .

As stated above, we consider a collision dynamics in two stages: the first was described in Ref. [18] and it consists of a sudden SEC by $\text{Sn}^{3+}(5s^2S)$ from $\text{H}_2(X^1\Sigma_g^+)$ at $R_i \approx 8$ bohr to produce $\text{Sn}^{2+}(5s5p^3P^0) + \text{H}_2^+(X^2\Sigma_g^+)$. In this stage, $\text{H}_2^+(X^2\Sigma_g^+)$ is formed in a fast transition that

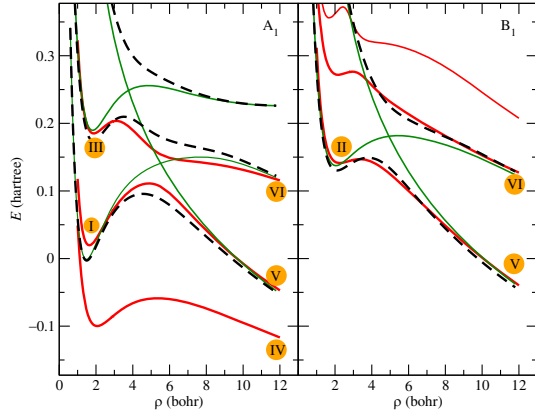


FIG. 2. Energies of the first five electronic states of the $(\text{Sn} + \text{H}_2)^{3+}$ system as functions of ρ for $R = 5$ bohr. Left panel: states $C_{2v} A_1$; right panel: states B_1 . Solid red thick lines are the *ab initio* data, thin green solid lines are the fitted diabatic states, and thick black dashed lines are the modeled adiabatic states. The character of adiabatic electronic states is: (I) $\text{Sn}^{3+}(5s^2S) + \text{H}_2(X^1\Sigma_g^+)$; (II) and (III) $\text{Sn}^{2+}(5s5p^3P^0) + \text{H}_2^+(X^2\Sigma_g^+)$; (IV) $\text{Sn}^{2+}(5s^2^1S) + \text{H}_2^+(X^2\Sigma_g^+)$; (V) $\text{Sn}^{2+}(5s^25p^2P^0) + 2\text{H}_2^+$; (VI) $\text{Sn}^{2+}(5s5p^3P^0) + \text{H}_2^+(X^2\Sigma_g^+)$.

preserves the vibrational wave function of H_2 . The probability of this first SEC is $P^{\text{SEC}} \approx 0.7$ (see Fig. 7 of Ref. [18]) and produces the population of the A_1 SEC state (i.e., capture into the $5p_z$ orbital). In the second stage of the collision, the newly formed H_2^+ undergoes a vibrational dynamics while the rotational couplings allow the population of the B_1 states from the A_1 ones.

The second stage of the collision is the focus of the present Letter. Here, we use the time-dependent Schrödinger equation (TDSE), $H\Psi = (T + V)\Psi = i\hbar\dot{\Psi}$ to propagate a multi-state 1D vibrational wave packet (WP) $\Psi(\rho, t) = (\Psi_1, \Psi_2, \Psi_3, \dots)$. T is the kinetic energy operator and $V[\rho, \mathbf{R}(t)]$ the potential energy that depends on t , since the interaction between the charged particles is a function of the coordinate $\mathbf{R}(t)$. The potential energy matrix V is expressed in a diabatic basis obtained by fitting the adiabatic PECs, calculated using the *ab initio* model of Ref. [18]. The nondiagonal blocks V_{kl} give rise to transitions that change the weights $\|\Psi_k\|^2$ of the different components of the WP. As mentioned, the WP propagation is performed by numerically solving the TDSE in a grid [36]. We use a second-order finite difference method with a time step of 0.01 a.u. The grid is a set of 250 equally spaced values of ρ in the interval 0.6 to 11.8 bohr. The kinetic energy T is calculated with a 5-point stencil. Unphysical bouncing on the grid limits is avoided using a mask function that fades away the WP for $\rho > 10.8$ bohr. The propagation starts after the sudden transition from the initial adiabatic PEC to that corresponding to the SEC channel (III) (see Fig. 2). The WP evolving in (III) is partially transferred to (II) by the rotational coupling. Both

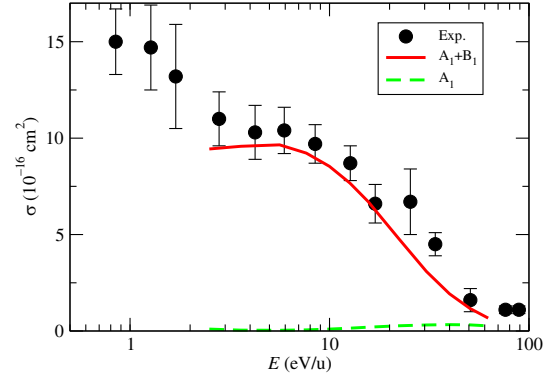


FIG. 3. Double electron capture cross sections as functions of the collision energy. Bullets, experimental values. Lines labeled A_1 and $A_1 + B_1$, results for $\sigma(A_1)$ and $\sigma(A_1) + \sigma(B_1)$.

channels, (II) and (III) show similar PEC profile for $\rho < 3$ bohr. The transitions in the vicinity of the crossings between the diabatic PECs yield DEC. For instance, at $R = 5$ bohr (Fig. 2), the crossings at $\rho \approx 4$ bohr produce two components of the WP that evolve on the dissociative PECs [labeled asymptotically as (V)] that lead to DEC. For each ion trajectory the DEC probability, is calculated from the probability density current that arrives to the grid limit. [36,37]. Multiplying the probabilities from the two stages of the mechanism, the probability for DEC at a given ion velocity and for each symmetry, S , is $P_S^{\text{SEC}}(z = z_i, b)P_S^{\text{DEC}}(b)$, where $z_i = (R_i^2 - b^2)^{1/2}$.

The main uncertainty of our model is the initial population of the SEC channel of B_1 symmetry. As already mentioned, it takes place from the corresponding one in the A_1 irreducible representation. The dynamical calculations [18] found similar populations of both SEC states at the point of closest approach and, accordingly, our model assumes initial probabilities $P_{A_1}^{\text{SEC}}(z_i, b) = P_{B_1}^{\text{SEC}}(z_i, b) = 1/2P^{\text{SEC}}(z_i, b)$, where $P^{\text{SEC}}(z_i, b)$ is the probability of SEC after the first stage at a given velocity and impact parameter.

In Fig. 3 we plot the experimental DEC cross sections as functions of the projectile energy, showing a sharp increase in magnitude as the collisional energy decreases from 50 to 10 eV/u. The solid line corresponds to the calculated data. The contribution of the A_1 subsystem is small and indicated with a dashed line. Furthermore, the electron capture of two electrons in one step, at short projectile-target distances, that is accounted for by the contribution to DEC from the channel (I) is negligible. The A_1 contribution to DEC is very small because the WP is trapped in the potential well [see (III) in Fig. 2] while the shallower well of the corresponding potential B_1 [(II) in Fig. 2] allows the spread of the WP that leads to DEC. Small changes in the distance (R_i) at which the first SEC takes place mainly shift the DEC cross sections to lower energies as R_i decreases or higher energies as R_i increases.

The good agreement between measured and calculated DEC cross sections, particularly in terms of their magnitude

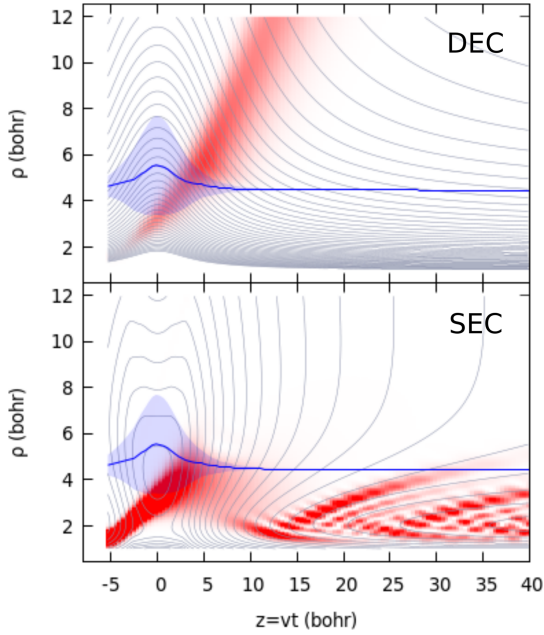


FIG. 4. Evolution of the probability density (red) $|\Psi_{\text{SEC}}|^2$ (bottom panel) and $|\Psi_{\text{DEC}}|^2$ (top panel) as a function of the z coordinate of the tin ion. The B_1 diabatic potential energy surfaces are shown as contour levels (grey lines). This propagation corresponds to $E = 10$ eV/u and $b = 4.0$ bohr. The blue solid line is the seam between the SEC and DEC potential energy surfaces, the width of blue shaded area is drawn proportional to the interaction matrix element between these states. An animation of the evolution of the two components of the WP is available as Supplemental Material [38].

and energy dependence, indicates that the model effectively captures the essential physics of DEC. However, at very low velocities ($E < 3$ eV/u) the interplay between electronic transitions and rotational motion, along with the limitations of the semiclassical approximation, may limit the validity of the model.

As a further illustration, we show in Fig. 4, the time evolution of the two components of the WP in the B_1 subsystem for $E = 10$ eV/u. The intensity of the shade in red is proportional to the components $|\Psi_i(\rho, t)|^2$ of the WP. Initially ($z \approx -5$ bohr), the WP is placed on the SEC surface (bottom panel), and has significant values only near $\rho = 1.4$ bohr. As the projectile advances along its trajectory, the WP spreads and its maximum shifts to larger values of ρ . In the region where the SEC and DEC diabatic surfaces intersect (blue line), the WP is partially transferred to the DEC surface. This transition is efficient only when the interaction matrix element is significant ($|z| \lesssim 5$ bohr in Fig. 4, blue-shaded region). Figure 5 shows the evolution of the WP for $E = 40$ eV/u. As the energy of projectile increases, the relatively slow motion of the WP prevents a significant portion of it from reaching the interaction region, resulting in a decrease in the DEC cross section. In both cases, it is also observed that the WP that remains in the SEC state bounces back from the potential energy

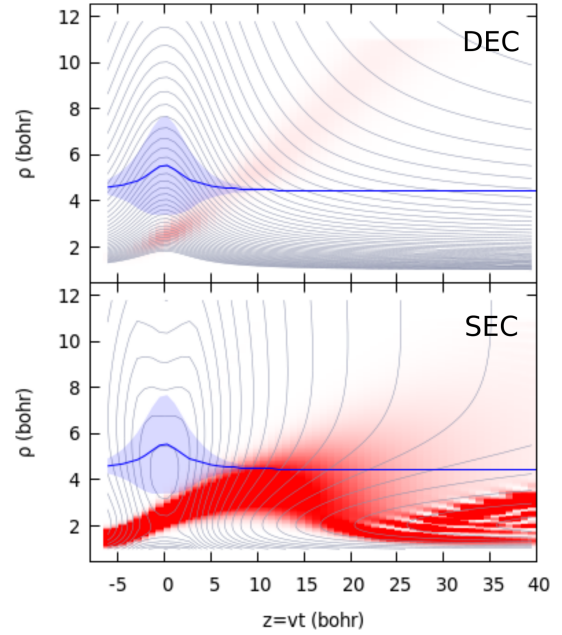


FIG. 5. Same as in Fig. 4, but for $E = 40$ eV/u.

barrier at $\rho \approx 5$ bohr, undergoing significant vibrational excitation. This is evident in the oscillations shown in the bottom panels at large z .

In summary, our experiments have revealed a remarkable high double electron capture cross sections in collisions of Sn^{3+} with H_2 , with values increasing as the impact energy decreases below 50 eV/u. To explain these results, we propose a two-step mechanism beyond the Franck-Condon approximation: initially, an electron capture at long projectile-target distances triggers the bond opening of H_2^+ . As the Sn^{2+} approaches, it modifies the shallow potential of H_2^+ , enabling it to reach a bond length of approximately 4 bohr. At that point, the second electron can be captured by the tin ion. The efficiency of this second electron capture depends on the balance between the time required for the H_2^+ bond to open and the time required by the tin ion to reach the target vicinity. This novel mechanism provides a valuable framework for understanding and designing experiments of double electron capture with other molecular targets. We anticipate that the two-step mechanism outlined in this Letter will exhibit varied signatures across different systems. For example, D_2 possesses a greater reduced mass compared to H_2 , resulting in a slower-moving target wave packet and requiring lower projectile energy to achieve equivalent DEC cross section values. Additionally, an intriguing case arises for targets where the first electron is ejected from an antibonding orbital, generating a wave packet that initially moves in the opposite direction compared to what occurs in the H_2 molecule.

Acknowledgments—The authors acknowledge the Centro de Computación Científica of UAM for computer hosting facilities. The experimental work was carried out at

the ZERNIKELEIF facility in the Zernike Institute for Advanced Materials of the University of Groningen as part of the research portfolio of the Advanced Research Center for Nanolithography (ARCNL), a public-private partnership between the University of Amsterdam (UvA), the Vrije Universiteit Amsterdam (VU), the University of Groningen (RuG), the Netherlands organization for Scientific Research (NWO), and the semiconductor equipment manufacturer ASML.

-
- [1] G. Van Eden, T. Morgan, D. Aussems, M. Van Den Berg, K. Bystrov, and M. Van De Sanden, Self-regulated plasma heat flux mitigation due to liquid Sn vapor shielding, *Phys. Rev. Lett.* **116**, 135002 (2016).
- [2] R. Nygren and F. Tabarés, Liquid surfaces for fusion plasma facing components—a critical review. Part I: Physics and PSI, *Nucl. Mater. Energy* **9**, 6 (2016).
- [3] G. Van Eden, V. Kvon, M. Van De Sanden, and T. Morgan, Oscillatory vapour shielding of liquid metal walls in nuclear fusion devices, *Nat. Commun.* **8**, 192 (2017).
- [4] W. Svendsen and G. O’Sullivan, Statistics and characteristics of XUV transition arrays from laser-produced plasmas of the elements tin through iodine, *Phys. Rev. A* **50**, 3710 (1994).
- [5] V. Y. Banine, K. Koshelev, and G. Swinkels, Physical processes in EUV sources for microlithography, *J. Phys. D* **44**, 253001 (2011).
- [6] G. O’Sullivan, B. Li, R. D’Arcy, P. Dunne, P. Hayden, D. Kilbane, T. McCormack, H. Ohashi, F. O’Reilly, P. Sheridan *et al.*, Spectroscopy of highly charged ions and its relevance to EUV and soft x-ray source development, *J. Phys. B* **48**, 144025 (2015).
- [7] O. O. Versolato, Physics of laser-driven tin plasma sources of EUV radiation for nanolithography, *Plasma Sources Sci. Technol.* **28**, 083001 (2019).
- [8] S. Fujioka, H. Nishimura, K. Nishihara, M. Murakami, Y.-G. Kang, Q. Gu, K. Nagai, T. Norimatsu, N. Miyanaga, Y. Izawa, K. Mima, Y. Shimada, A. Sunahara, and H. Furukawa, Properties of ion debris emitted from laser-produced mass-limited tin plasmas for extreme ultraviolet light source applications, *Appl. Phys. Lett.* **87**, 241503 (2005).
- [9] A. Bayerle, M. J. Deuzeman, S. van der Heijden, D. Kurilovich, T. de Faria Pinto, A. Stodolna, S. Witte, K. S. E. Eikema, W. Ubachs, R. Hoekstra, and O. O. Versolato, Sn ion energy distributions of ns- and ps-laser produced plasmas, *Plasma Sources Sci. Technol.* **27**, 045001 (2018).
- [10] L. Poirier, A. Bayerle, A. Lassise, F. Torretti, R. Schupp, L. Behnke, Y. Mostafa, W. Ubachs, O. O. Versolato, and R. Hoekstra, Cross-calibration of a combined electrostatic and time-of-flight analyzer for energy- and charge-state-resolved spectrometry of tin laser-produced plasma, *Appl. Phys. B* **128**, 39 (2022).
- [11] D. Nakamura, K. Tamaru, Y. Hashimoto, T. Okada, H. Tanaka, and A. Takahashi, Mitigation of fast ions generated from laser-produced Sn plasma for extreme ultraviolet light source by H₂ gas, *J. Appl. Phys.* **102**, 123310 (2007).
- [12] I. Fomenkov, D. Brandt, A. Ershov, A. Schafgans, Y. Tao, G. Vaschenko, S. Rokitski, M. Kats, M. Vargas, M. Purvis, R. Rafac, B. L. Fontaine, S. D. Dea, A. LaForge, J. Stewart, S. Chang, M. Graham, D. Riggs, T. Taylor, M. Abraham, and D. Brown, Light sources for high-volume manufacturing EUV lithography: Technology, performance, and power scaling, *Adv. Opt. Technol.* **6**, 173 (2017).
- [13] S. Rai, K. I. Bijlsma, L. Poirier, E. de Wit, L. Assink, A. Lassise, I. Rabadán, L. Méndez, J. Sheil, O. O. Versolato, and R. Hoekstra, Evidence of production of keV Sn⁺ ions in the H₂ buffer gas surrounding an Sn-plasma EUV source, *Plasma Sources Sci. Technol.* **32**, 035006 (2023).
- [14] D. B. Abramenko, M. V. Spiridonov, P. V. Krainov, V. M. Krivtsun, D. I. Astakhov, V. V. Medvedev, M. van Kampen, D. Smeets, and K. N. Koshelev, Measurements of hydrogen gas stopping efficiency for tin ions from laser-produced plasma, *Appl. Phys. Lett.* **112**, 164102 (2018).
- [15] Y. I. M. Imai and A. Itoh, Target dependence of single-electron-capture cross sections for slow Be, B, C, Fe, Ni, and W ions colliding with atomic and molecular targets, *Fusion Sci. Technol.* **63**, 392 (2013).
- [16] R. A. Lomsadze, M. R. Gochitashvili, and R. Y. Kezerashvili, Inelastic processes in Na⁺-Ne, Na⁺-Ar, Ne⁺-Na, and Ar⁺-Na collisions in the energy range 0.5–14 keV, *Phys. Rev. A* **92**, 062703 (2015).
- [17] K. Bijlsma, L. Oltra, E. de Wit, L. Assink, I. Rabadán, L. Méndez, and R. Hoekstra, Electron capture from molecular hydrogen by metastable Sn²⁺⁺ ions, *Atoms* **12**, 9 (2024).
- [18] S. Rai, K. I. Bijlsma, I. Rabadán, L. Méndez, P. A. J. Wolff, M. Salverda, O. O. Versolato, and R. Hoekstra, Charge exchange in collisions of 1–100 keV Sn³⁺ ions with H₂ and D₂, *Phys. Rev. A* **106**, 012804 (2022).
- [19] J. R. Machacek, D. P. Mahapatra, D. R. Schultz, Y. Ralchenko, A. Chutjian, J. Simcic, and R. J. Mawhorter, Measurement and calculation of absolute single- and double-charge-exchange cross sections for O⁶⁺ ions at 1.17 and 2.33 keV/u impacting He and H₂, *Phys. Rev. A* **90**, 052708 (2014).
- [20] K. Bijlsma, Electron capture in collisions of tin ions with molecular hydrogen, Ph.D. thesis, University of Groningen, 2024, 10.33612/diss.1001345207.
- [21] L. F. Errea, J. D. Gorfinkiel, A. Macías, L. Méndez, and A. Riera, Charge transfer and dissociation in C^{q+} + H₂ collisions, *Phys. Scr.* **1999**, 185 (1999).
- [22] L. F. Errea, J. D. Gorfinkiel, C. Harel, H. Jouin, A. Macías, L. Méndez, B. Pons, and A. Riera, Model potential treatment of C⁴⁺ + H₂ collisions at low impact energies, *J. Phys. B* **33**, 3107 (2000).
- [23] B. Zarour, C. Champion, J. Hanssen, and B. Lasri, Charge transfer and dissociation of H₂ molecule in slow collisions with C⁴⁺ ions, *Nucl. Instrum. Methods Phys. Res., Sect. B* **235**, 374 (2005).
- [24] L. F. Errea, A. Macías, L. Méndez, B. Pons, and A. Riera, Molecular treatment of single (dissociative and nondissociative) and double electron capture in He²⁺ + H₂ collisions, *J. Phys. B* **36**, L135 (2003).
- [25] L. F. Errea, A. Macías, L. Méndez, B. Pons, and A. Riera, Quantum chemistry calculation of excited three center systems: Theoretical study of He²⁺ + H₂ collisions, *J. Chem. Phys.* **119**, 325 (2003).

- [26] J. W. Gao, Y. Y. Qi, Y. Wu, and J. G. Wang, Single- and double-electron capture cross sections for O^{6+} ion in collisions with H_2 molecules, *Astrophys. J.* **944**, 167 (2023).
- [27] K. Soejima, C. J. Latimer, K. Okuno, N. Kobayashi, and Y. Kaneko, Cross sections for single and multiple electron capture in low energy collisions of C^{4+} with H_2 , O_2 and N_2 , *J. Phys. B* **25**, 3009 (1992).
- [28] A. Itoh, N. Imanishi, F. Fukuzawa, N. Hamamoto, S. Hanawa, T. Tanaka, T. Ohdaira, M. Saito, Y. Haruyama, and T. Shirai, Single-, double- and triple-electron capture cross sections for multicharged slow carbon ions in H_2 , CH_4 , C_2H_6 , C_3H_8 and CO_2 molecules, *J. Phys. Soc. Jpn.* **64**, 3255 (1995).
- [29] T. Kusakabe, H. Yoneda, Y. Mizumoto, and K. Katsurayama, Charge transfer cross sections of $^3He^{2+}$ ions in collisions with He atoms and H_2 molecules in the energy range of 1–10 keV, *J. Phys. Soc. Jpn.* **59**, 1218 (1990).
- [30] K. Okuno, K. Soejima, and Y. Kaneko, Single- and double-electron capture in $^3He^{2+}$ - H_2 collisions at low energies from 1 to 2000 eV, *J. Phys. B* **25**, L105 (1992).
- [31] Z. Juhász, G. Lubinski, R. Morgenstern, and R. Hoekstra, Line emission spectroscopy of low-energy charge transfer reactions, *At. Plasma-Mater. Interact. Data Fusion* **10**, 25 (2002), <https://www.iaea.org/publications/6618/atomic-and-plasma-material-interaction-data-for-fusion>.
- [32] J. B. Greenwood, I. D. Williams, S. J. Smith, and A. Chutjian, Experimental investigation of the processes determining x-ray emission intensities from charge-exchange collisions, *Phys. Rev. A* **63**, 062707 (2001).
- [33] J. P. Giese, C. L. Cocke, W. T. Waggoner, J. O. K. Pedersen, E. Y. Kamber, and L. N. Tunnell, Non-Franck-Condon transitions in two-electron capture from D_2 by low-energy, highly charged Ar projectiles, *Phys. Rev. A* **38**, 4494 (1988).
- [34] C. J. Wood and R. E. Olson, Double electron removal and fragmentation model of the H_2 molecule by highly charged ions, *Phys. Rev. A* **59**, 1317 (1999).
- [35] R. D. DuBois, T. Schlathölter, O. Hadjar, R. Hoekstra, R. Morgenstern, C. M. Doudna, R. Feeler, and R. E. Olson, Molecular fragmentation by slow highly charged ion impact, *Europhys. Lett.* **49**, 41 (2000).
- [36] J. Suárez, L. Méndez, and I. Rabadán, Nonadiabatic quantum dynamics predissociation of $H_2O^+(\tilde{B}^2B_2)$, *J. Phys. Chem. Lett.* **6**, 72 (2015).
- [37] I. Benito-Gómez, L. Méndez, J. Suárez, J. D. Gorfinkiel, and I. Rabadán, Resonant fragmentation of the water cation by electron impact: A wave-packet study, *ChemPhysChem* **24**, e202300305 (2023).
- [38] See Supplemental Material at <http://link.aps.org/supplemental/10.1103/PhysRevLett.134.093002> for the animation of the two components (DEC and SEC) of the WP on the B_1 electronic states.